Supplementary Material

1 Supplementary Text

1.1 Flux-gradient modelling of soil CO_2 fluxes

1.1.1 Calculation of soil CO_2 profiles

For a homogeneous layer of soil with a constant production rate P, the flux F at any height z of the layer (measured from the bottom of the layer) is the integral of P over z. This applies for steady state conditions under the assumption that the produced CO_2 is only removed in one direction (as efflux from the surface),

$$F(z) = \int_0^z P dz = P \cdot z + F_{\text{in}} \tag{1}$$

where F_{in} is the incoming flux at the bottom of the layer.

The CO_2 flux F [µmol m^{-2} s^{-1}] through a soil layer with a given effective soil diffusion coefficient D_S [m^2 s^{-1}] at steady state must suffice Ficks's first law:

$$F(z) = -D_s \frac{dc}{\mathrm{d}z} \tag{2}$$

where D_s is the effective soil diffusion coefficient [m^2 s^{-1}] as a function of the free air CO_2 diffusion coefficient under standard conditions, D_0^{ref} (1.369*10^{-5} m^2 s^{-1} at T_{ref} =273.15 K and p_{ref} =101325 Pa), corrected by air temperature (T_a) and air pressure (p_a) according to (Maier and Schack-Kirchner, 2014) as:

$$D_s = D_r \cdot D_0(T_a, p_a) \cdot \left(\frac{T_a}{T_{\text{ref}}}\right)^{1.9206} \cdot \left(\frac{p_{\text{ref}}}{p_a}\right) \tag{3}$$

Equating (1) and (2), solving for the concentration gradient $\frac{dc}{dz}$ yields:

$$P \cdot z + F_{\text{in}} = -D_s \frac{dc}{\mathrm{d}z} \tag{4}$$

$$\frac{dc}{\mathrm{d}z} = -\frac{P}{D_s} \cdot z - \frac{F_{in}}{D_s} \tag{5}$$

Finally, we integrated again over z to provide a formula for the concentration depending on the height z above the bottom of the layer.

$$c(z) = -\frac{P}{2D_s}z^2 - \frac{F_{\text{in}}}{D_s}z + c_0 \quad (6)$$

It can be seen that a positive production rate within a layer (P) or a positive influx at the bottom of the layer (F_{in}) results in a decrease of $c(z)$ from the concentration c_0 at the bottom to the top of the layer.

For a given soil profile at any time step, these equations are solved for each layer "bottom up" requiring a known CO_2 concentration c_0 at the bottom of the lowest layer. The influx into the lowest layer can be assumed to be zero if the layer is deep enough (zero-flux boundary condition). Based on this, the concentration c_1 and flux F_1 at the top of the layer can be calculated. F_1 and c_1 correspond to F_{in} and c_0 of the layer above. This way, soil CO_2 profiles can be calculated layer by layer from bottom to top based on assumed CO_2 production rates and D_s. The upper and lower limits of allowed production rates per layer were set uniformly to 1,000 and 0 μmol m^{-3} s^{-1}.

1.1.2 Vertical partitioning of soil respiration by inverse modelling

To derive the vertical production profile at any time step an inverse model was applied. This was achieved by using the "L-BFGS-BS" algorithm (Byrd et al., 1995), implemented in R Stats Package. The model was implemented in R 4.0.2 (R-Core-Team, 2020) using dplyr 1.0.7 (Wickham et al., 2021). An objective function was set up that calculates an error-parameter to be minimised by the algorithm. The basic error parameter is a weighted root mean square error (RMSE) of the calculated concentration (c_{model}) to the concentration measurement(s) (c_{measured}) at each depth.

$$RMSE = \sqrt{\frac{1}{n} * \sum_{i=1}^{n} \left(f_i * \left(c_{measured,i} - c_{model,i}\right)^2\right)} \quad (7)$$

where n = number of unique observations i, and f_i = weighting factor. Each square error i is weighted with a factor f_i to account for differences in the number of measurements at each depth and for the different degrees of freedom each modelled concentration depends on. The weighting factor f_i is calculated by:

$$f_i = \frac{k^2}{n_k} \quad (8)$$

where k = number of degrees of freedom (different production rates) from the deepest layer to the respective depth, and n_k = number of observations within the respective production layer. The RMSE is then scaled to the mean concentration in the profile (based on the measurements).

$$RMSE_s = \frac{RMSE}{mean(c_{measured})} \quad (9)$$

To reduce the exceptionally large spreading of the optimized production rates within a profile, a penalisation was applied (PEN_e). Here, a very low production rate is inversely penalised, depending on the maximum production rate of the profile (P_{max}) and a user-defined evenness factor (f_e). The

height or thickness of each layer, h_k is used to weigh the contribution of the production P_k of the respective layer to the PEN_e of the profile.

$$PEN_e = f_e * \frac{1}{n(k)} * \sum_{k=1}^{n(k)} \frac{(P_{max})^2}{|\frac{P_k}{h_k}|} \quad (10)$$

The final objective term ($RMSE_p$) is the sum of $RMSE_s$ and the penalisation PEN_e that is minimised by the algorithm.

$$RMSE_p = RMSE_s + PEN_e \quad (11)$$

For each profile, four independent production rates at four soil layers (O horizon, A horizon, B to 30 cm, B 30 to 100 cm) were optimised using the method described above.

1.1.3 Identification of effective soil physical properties

Measurements of soil physical properties have inherent methodological uncertainties and spatial variability. Although measurement repetitions may help assess these uncertainties, the resulting mean value can deviate from an effective representative value that would best describe actual conditions. Instead of using the arithmetic mean values of the replicate measurements of soil physical properties, we tested several sets of parameters to find a model parameterisation that a) best predicted the efflux at the soil-atmosphere interface and b) best fitted the concentration profiles.

Total pore space (TPS) of the humus layer, Ah and B horizons were varied between 85% and 110% the original parameterisation of the model alongside the thickness of the humus layer between 4 and 8 cm. A subset of 500 randomly chosen time-points was used, where soil profile data and chamber measurements were available, to limit computer runtime. Two error parameters were calculated using the data from the days with chamber measurements for the efflux validation ($NRMSE_{flux}$) and the random set for the concentration validation ($NRMSE_{conc}$). The parameters were calculated as follows. In the case of $NRMSE_{conc}$, *RMSE* of each level k (0, 10, 20, 30 cm soil depth) were first normalised individually and subsequently averaged to account for higher concentrations at a lower depth.

$$NRMSE_{conc} = \frac{1}{n(k)} * \sum_{k=1}^{n(k)} \frac{\sqrt{\frac{1}{n} * \sum_{i=1}^{n} (c_{meas,i} - c_{mod,i})^2}}{c_{max,k} - c_{min,k}} \quad (12)$$

$$NRMSE_{flux} = \sqrt{\frac{1}{n} * \sum_{i=1}^{n} \frac{(F_{c,i} - F_{mod,i})^2}{F_{max} - F_{min}}} \quad (13)$$

The 10 parameter sets with the smallest *NRMSE* values were chosen for each site and repeated by the simple addition of the $NRMSE_{flux}$ and $NRMSE_{conc}$ after normalisation with the respective range of values of $NRMSE_{conc}/NRMSE_{flux}$. From these, the set with the least deviation from the original parameter-set was chosen for further modelling. These final parameter sets are shown in (Supplementary Table 1).

Additionally, a second sweep was performed using the same profiles and using the optimised parameter sets shown in (Supplementary Table 1) to find the best value for the evenness-penalisation,

the evenness-factor f_{even}. Here, the lowest factor that would limit the number of time points with values of zero production while maintaining a good fit with chamber-fluxes and CO_2 concentration profiles were chosen. The value was set to $f_{even} = 0.0001$ for both beech and pine.

1.1.4 Assumptions and limitations for modelling of soil CO_2 fluxes using effective soil physical parameters

Several approaches have been developed to calculate soil-atmosphere fluxes using the FGM and derive vertical CO_2 production profiles (Maier and Schack-Kirchner, 2014). De Jong and Schappert (1972) and several other authors, e.g. (Tang et al., 2003; Hirano, 2005; Tang et al., 2005; Maier et al., 2010) calculated fluxes based on discrete gradients. Since we were interested in investigating the development of the vertical production profiles, we followed a different approach and derived the flux and production profiles through inverse modelling. This means the soil gas profiles were (forward) calculated based on theoretical profiles of production and diffusivity of soil gas. In a second step, an optimisation algorithm was used to adapt the production profile to fit the measured soil gas profile. This approach allowed explicit constraints, such as limiting the possible CO_2 production in each layer and the condition that CO_2 is not consumed in relevant amounts in the soil. However, the penalisation factors and other input parameters affect the final vertical production profile, and a different parameterisation could lead to a slightly different result.

We used chamber measurements as an additional reference value for the FGM estimated efflux, as has been done in other studies using chamber-based flux estimates to assess topsoil diffusivity (Koehler et al., 2010; Sánchez-Cañete et al., 2017) or humus layer CO_2 production (Davidson et al., 2006). We performed parameter-sweeps for the total pore space of all soil layers and the thickness of the humus layer to identify the most suitable set of parameter values within the observed variability of our soil physical measurements. Using the chamber measurements as an additional reference provided a better estimate of plausible effective parameter combinations.

We found that the thickness of the humus layer has an effect on the FGM-derived efflux (see Supplement). The humus layer is usually exposed to intense drying and wetting cycles, which are rarely studied. Some studies completely excluded the humus layer from the FGM (Davidson et al., 2006; Wordell-Dietrich et al., 2020), and very few studies systematically analysed soil gas diffusivity in the humus layer (Maier and Lang, 2019). Moreover, CO_2 exchange through the humus layer can be affected by wind. The coarse L layer allows CO_2 to accumulate in calm situations but is easily flushed subsequently by small wind gusts (Novak et al., 2000; Hirsch et al., 2004; Maier et al., 2012). As a result, the effective thickness of the humus layer can easily have an uncertainty of 2 – 3 cm for a thickness of 5 cm on average.

Since the modelling parameters were set after the effective soil physical parameters were optimised for the entire time course of the data, the modelled temporal evolution of CO_2 fluxes and production in soil were determined only by the measured data. The modelling results of the parameter sweeps showed that the temporal evolution of fluxes was very consistent for all tested parameter sets while the vertical partitioning and efflux changed slightly (data not shown). The selected set of effective soil physical parameters not only provided a good quality of fit for the concentration profile and the efflux estimates but also showed a good agreement with root density profiles at both sites (see main text Figure 4).

1.2 **Simulation of soil water contents using HYDRUS-1D**

The soil water contents of the organic layer (O) horizons of the two sites, which could not be directly measured, were obtained from results of numerical soil water balance simulations using the well-known HYDRUS-1D program (version 4.17.0140, Šimůnek et al. (2009)). Only the main approaches and methods are described here because a complete description of the forest water balance was beyond the scope of this study.

In the HYDRUS program, the Richards' equation for variably-saturated water movement in soil is numerically solved with a finite element scheme. The soil hydraulic parameters are described with the standard constraint van Genuchten-Mualem (vGM) functions. For the O-horizons, the vGM-parameters (α, n, θ_s, θ_r, K_s, ℓ=0.5, m=1-1/n) were estimated; for the mineral soil horizons, the vGM parameters were first taken from soil core data and then fitted to better match the measured water contents (see Supplementary Table 3 for a list of parameter values). The spatial discretisation of the numerical grid was 1 cm and the time stepping was max. 0.5 hours. At the soil surface, atmospheric and at the bottom, free drainage boundary conditions were imposed.

The potential evapotranspiration (PET) was calculated from meteorological data (i.e., air temperature, mean relative air humidity, solar radiation, air pressure, and open field precipitation at an hourly temporal resolution, all in 2 m height, and wind velocity in 10 m). The PET was calculated according to ASCE Standardized Reference Evapotranspiration Equation (ASCE-EWRI, 2005), which is based on the Penman-Monteith equation (Allen et al., 1998) with stomatal and bulk resistance values according to Allen et al. (2006). In the sink term of the Richards' equation, the root water uptake was described by a water stress response function (Feddes et al., 1978). The vertical root density distribution (see main text Table 1) was assumed constant.

For calculating the soil water infiltration, the open field precipitation and canopy interception data were used. The canopy interception calculations were based on the leaf area index (LAI), which was measured using LAI-2000 Plant Canopy Analyzer (Li-Cor Biosciences). Start and end of the vegetation (i.e., leaf unfolding and litterfall), was determined for the beech site from the radiation difference between the open field and the stand below the canopy; for the pine stand, it was determined from canopy photos taken by a webcam. For the pine stand, the LAI of the blueberry vegetation was considered additive to that of the pine trees. The canopy factor in the HYDRUS program was assumed constant, with 0.61 for beech and 0.51 for pine. The interception constant was a = 0.025 mm.

The simulation period covered all years of this study (2014–2019). The initial water content profile was obtained from linearly interpolated *SWC* data at observation points. Simulation results were compared with measured *SWC* values and soil matric potential data at the corresponding soil depths.

References

Allen, R.G., Pereira, L.S., Raes, D., and Smith, M. (1998). *Crop evapotranspiration - Guidelines for computing crop water requirements -.* Rome: FAO - Food and Agriculture Organization of the United Nations.

Allen, R.G., Pruitt, W.O., Wright, J.L., Howell, T.A., Ventura, F., Snyder, R., Itenfisu, D., Steduto, P., Berengena, J., Yrisarry, J.B., Smith, M., Pereira, L.S., Raes, D., Perrier, A., Alves, I., Walter, I., and Elliott, R. (2006). A recommendation on standardized surface resistance for hourly calculation of reference ETo by the FAO56 Penman-Monteith method. Agricultural Water Management 81**,** 1-22. doi: 10.1016/j.agwat.2005.03.007

Byrd, R.H., Lu, P., Nocedal, J., and Zhu, C. (1995). A limited memory algorithm for bound constrained optimization. SIAM Journal on Scientific Computing 16**,** 1190-1208. doi: 10.1137/0916069

Davidson, E.A., Savage, K.E., Trumbore, S.E., and Borken, W. (2006). Vertical partitioning of CO_2 production within a temperate forest soil. Global Change Biology 12**,** 944-956. doi: 10.1111/j.1365-2486.2006.01142.x

De Jong, E., and Schappert, H.J.V. (1972). Calculation of soil respiration and activity from CO_2 profiles in the soil. Soil Science 113**,** 328-333. doi: 10.1097/00010694-197205000-00006

Feddes, R.A., Kowalik, P.J., and Zaradny, H. (1978). *Simulation of field water use and crop yield.* Wageningen: Centre for agricultural publishing and documentation.

Hirano, T. (2005). Seasonal and diurnal variations in topsoil and subsoil respiration under snowpack in a temperate deciduous forest. Global Biogeochemical Cycles 19. doi: 10.1029/2004gb002259

Hirsch, A.I., Trumbore, S.E., and Goulden, M.L. (2004). The surface CO_2 gradient and pore-space storage flux in a high-porosity litter layer. Tellus 56B**,** 312-321. doi: 10.3402/tellusb.v56i4.16449

Koehler, B., Zehe, E., Corre, M.D., and Veldkamp, E. (2010). An inverse analysis reveals limitations of the soil-CO_2 profile method to calculate CO_2 production and efflux for well-structured soils. Biogeosciences 7**,** 2311-2325. doi: 10.5194/bg-7-2311-2010

Maier, M., and Lang, V. (2019). Gas Diffusivity in the Forest Humus Layer. Soil Science 184**,** 13-16. doi: 10.1097/ss.0000000000000245

Maier, M., and Schack-Kirchner, H. (2014). Using the gradient method to determine soil gas flux: A review. Agricultural and Forest Meteorology 192-193**,** 78-95. doi: 10.1016/j.agrformet.2014.03.006

Maier, M., Schack-Kirchner, H., Aubinet, M., Goffin, S., Longdoz, B., and Parent, F. (2012). Turbulence effect on gas transport in three contrasting forest soils. Soil Science Society of America Journal 76**,** 151-1528. doi: 10.2136/sssaj2011.0376

Maier, M., Schack-Kirchner, H., Hildebrand, E.E., and Holst, J. (2010). Pore-space CO_2 dynamics in a deep, well-aerated soil. European Journal of Soil Science 61**,** 877-887. doi: 10.1111/j.1365-2389.2010.01287.x

Novak, M.D., Chen, W., Orchansky, A.L., and Ketler, R. (2000). Turbulent exchange processes within and above a straw mulch.: Part I: Mean wind speed and turbulent statistics. Agricultural and Forest Meteorology 102**,** 139-154. doi: 10.1016/S0168-1923(00)00095-2

R-Core-Team (2020). "A language and environment for statistical computing". (Vienna, Austria: Foundation for Statistical Computing).

Sánchez-Cañete, E.P., Scott, R.L., Haren, J.V., and Barron-Gafford, G.A. (2017). Improving the accuracy of the gradient method for determining soil carbon dioxide efflux. Journal of Geophysical Research: Biogeosciences 122**,** 50-64. doi: 10.1002/2016JG003530

Šimůnek, J., Šejna, M., Saito, H., Sakai, M., and Genuchten, M.T.V. (2009). "The HYDRUS-1D software package for simulating the one-dimensional movement of water, heat, and multiple solutes in variably-saturated media - Version 4.08". Department of Environmental Sciences, University of California, Riverside, California.

Tang, J., Baldocchi, D.D., Qi, Y., and Xu, L. (2003). Assessing soil CO_2 efflux using continuous measurements of CO_2 profiles in soils with small solid-state sensors. Agricultural and Forest Meteorology 118**,** 207-220. doi: 10.1016/S0168-1923(03)00112-6

Tang, J., Baldocchi, D.D., and Xu, L. (2005). Tree photosynthesis modulates soil respiration on a diurnal time scale. Global Change Biology 11**,** 1298-1304. doi: 10.1111/j.1365-2486.2005.00978.x

Wickham, H., François, R., Henry, L., and Müller, K. (2021). "dplyr: A grammar of data manipulation".

Wordell-Dietrich, P., Wotte, A., Rethemeyer, J., Bachmann, J., Helfrich, M., Kirfel, K., Leuschner, C., and Don, A. (2020). Vertical partitioning of CO_2 production in a forest soil. Biogeosciences 17**,** 6341-6356. doi: 10.5194/bg-17-6341-2020

2 Supplementary Tables and Figures

2.1 Supplementary Tables

Supplementary Table 1. Parameterisation of the inverse model regarding limits of soil depths of the O horizon and total pore space (TPS). The high and low limits of production rate were set uniformly to 1,000 and 0 µmol m^{-3} s^{-1}. Numbers in bold mark parameters deviating from measured ones.

Site	Plot	Upper depth [cm]	Lower depth [cm]	TPS
Beech	1	**7**	0	0.827
		0	-8	0.562
		-8	-30	**0.374**
		-30	-100	**0.374**
Beech	2	5	0	**0.785**
		0	-8	**0.478**
		-8	-30	0.440
		-30	-100	0.440
Beech	3	**6**	0	**0.785**
		0	-8	**0.478**
		-8	-30	0.440
		-30	-100	0.440
Pine	1	**7**	0	**0.888**
		0	-10	**0.645**
		-10	-30	**0.360**
		-30	-100	**0.360**
Pine	2	6	0	**0.888**
		0	-10	0.679
		-10	-30	**0.360**
		-30	-100	**0.360**
Pine	3	6	0	**0.888**
		0	-10	**0.747**
		-10	-30	**0.381**
		-30	-100	**0.381**

Supplementary Table 2. Soil hydraulic parameters used in the soil numerical soil water simulations.

Site	Horizon	Soil depth (cm)	θ_r $cm^3\ cm^{-3}$	θ_s $cm^3\ cm^{-3}$	α cm^{-1}	n -	K_s $cm\ d^{-1}$
Beech	O	4 – 0	0.137	0.860	0.0360	2.609	500.0
	A(e)h	0 – -7	0.011	0.619	0.0251	2.741	427.2
	Bhv	-7 – -32	0.051	0.394	0.0339	3.528	520.6
	Bv	-32 – -70	0.040	0.473	0.0371	2.930	619.9
	CI	-70 – -130	0.046	0.386	0.0339	4.006	770.9
	CII	-130 – -180	0.042	0.375	0.0328	4.035	847.2
Pine	O	6 – 0	0.140	0.860	0.0227	4.764	500.0
	Ahe	0 – -10	0.063	0.466	0.0348	2.639	273.0
	Bs	-10 – -35	0.033	0.484	0.0292	3.424	273.0
	Bsv	-35 – -60	0.022	0.397	0.0414	2.624	611.0
	C1	-60 – -65	0.021	0.409	0.0523	2.607	626.3
	C2	-65 – -95	0.021	0.409	0.0414	2.623	626.3
	Go	-95 – -170	0.021	0.424	0.0233	2.783	626.3

Supplementary Table 3. Mean soil CO_2 concentrations (ppmv) at both forest sites. Different lowercase letters indicate significant differences between the two forest sites according to the Wilcoxon test ($p < 0.05$). Different greek letters indicate significant differences between the soil layers according to the Friedman's test ($p < 0.05$).

Site	Soil depth	CO_2 [ppmv]
Beech	Surface	$451^{a\alpha}$
	0 cm	$1059^{a\beta}$
	-10 cm	$2300^{a\gamma}$
	-20 cm	$2867^{a\delta}$
	-30 cm	$3137^{a\varepsilon}$
	-100 cm	$4481^{a\zeta}$
Pine	Surface	$471^{b\alpha}$
	0 cm	$970^{b\beta}$
	-10 cm	$1486^{b\gamma}$
	-20 cm	$1837^{b\delta}$
	-30 cm	$2342^{b\varepsilon}$
	-100 cm	$3655^{b\zeta}$

2.2 **Supplementary Figures**

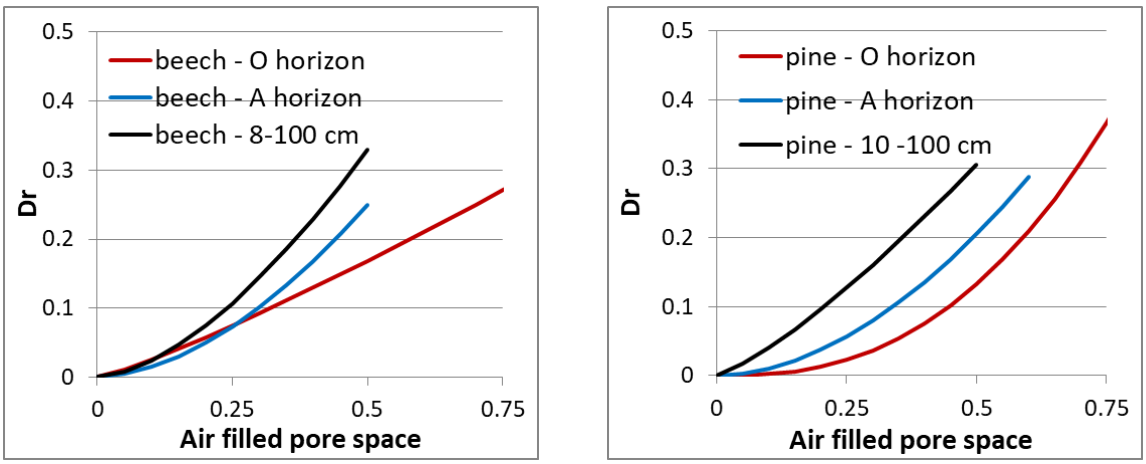

Supplementary Figure 1: Relative soil gas diffusion coefficients (D_r) for the beech site (left) and the pine site (right) as a function of air-filled pore space.

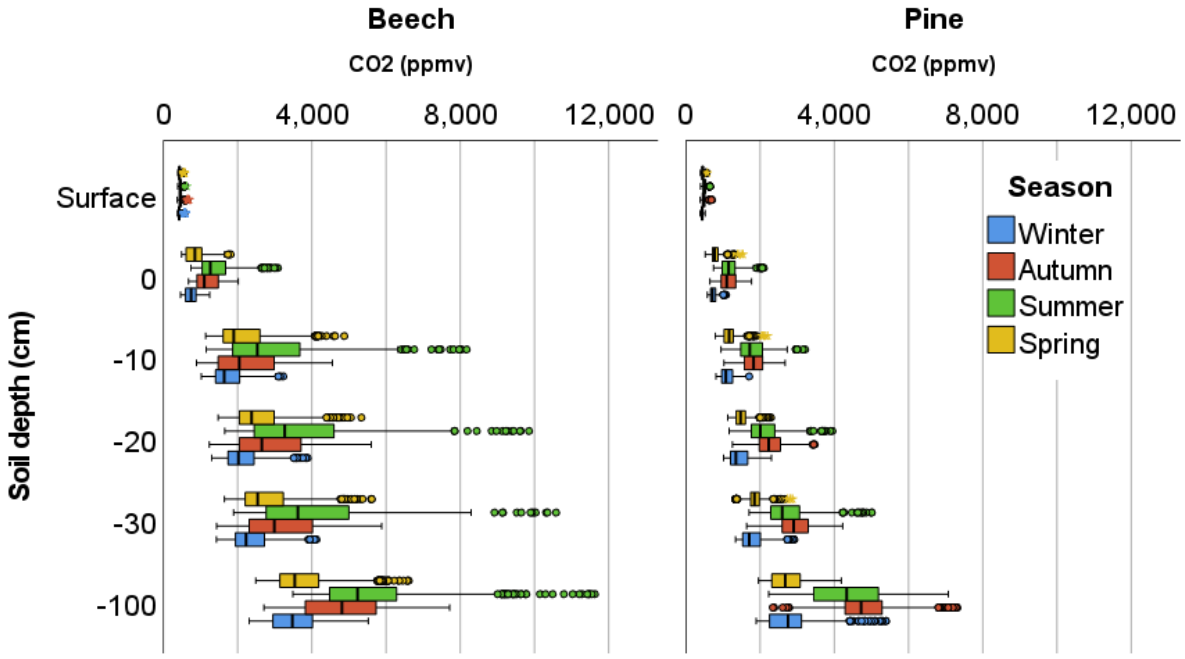

Supplementary Figure 2: Vertical distribution of daily averages of measured CO_2 concentrations at different soil depths of the beech and pine forests during spring (month 3–5), summer (6–8), autumn (9–11), and winter (12–2)

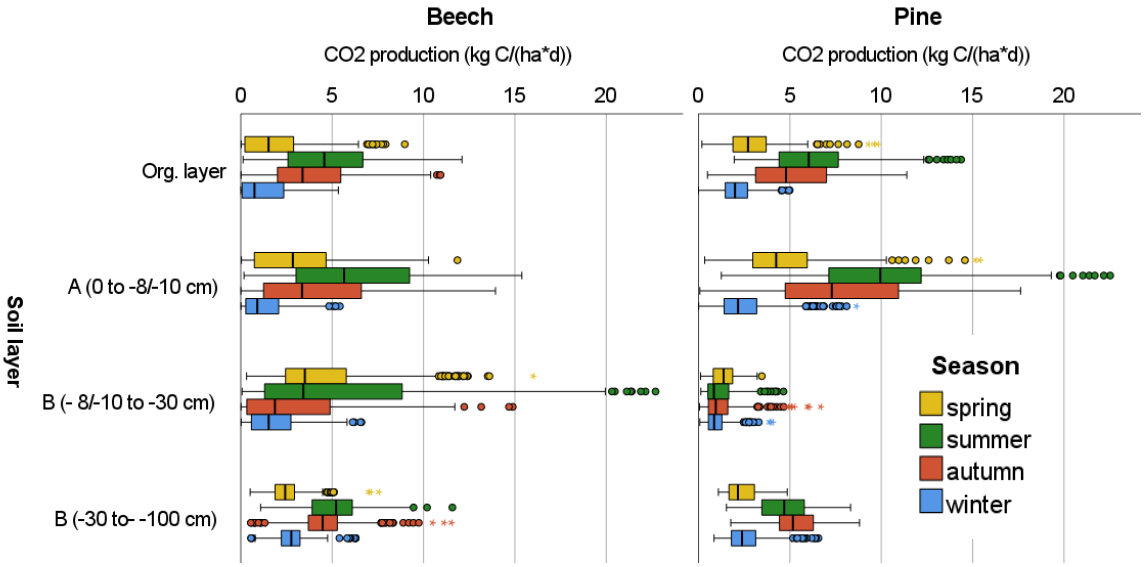

Supplementary Figure 3: Vertical distribution of layer-specific CO_2 production in soils of the beech (left) and pine (right) forests during spring (month 3–5), summer (6–8), autumn (9–11), and winter (12–2)

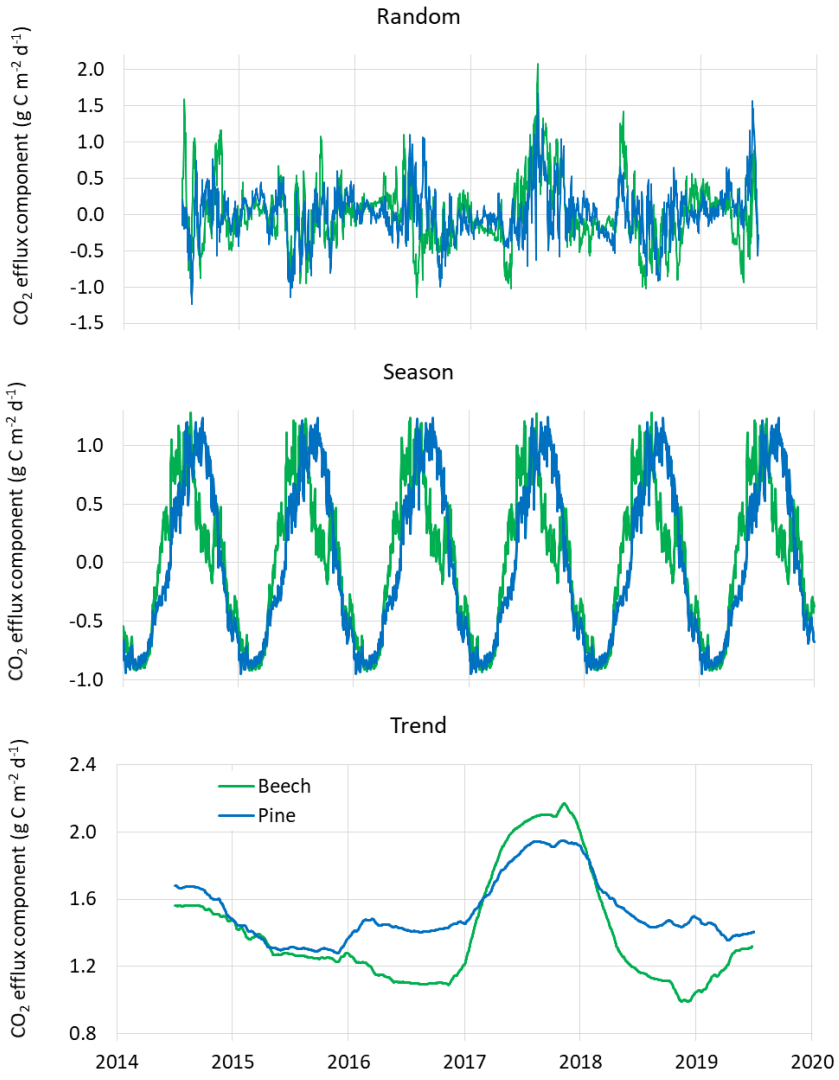

Supplementary Figure 4: Time series decomposition of CO_2 efflux into random, seasonal and trend components for the beech and the pine site